Journal of Mechanical Engineering and Applied Technology, Vol 4 (2) 2026, 123-136
e-ISSN : 3025-2725

# Beyond a Single Damping Coefficient: Experimental Mapping of Nonlinear and Stroke-Dependent Automotive Shock-Absorber Behaviour

**Avicenna An-Nizhami***, **Ignatius Gunawan Widodo, Muhammad Showi Nailul Ulum, Elfrida Rizky Riadini, Ahmad Mamba'udin, Yuris Bahadur Wirawan**

Departemen of Mechanical Engineering, Politeknik Negeri Semarang
Jl. Prof. Soedarto, Tembalang, Kec. Tembalang, Kota Semarang, Jawa Tengah, Indonesia
*E-mail: avicenna@polines.ac.id

Submitted: July 1, 2026; Accepted: July 23, 2026; Published: July 25, 2026

***Abstract***

*Shock absorbers are commonly represented by a constant viscous damping coefficient, although their actual force response may vary nonlinearly with piston velocity, stroke amplitude, and operating conditions. This study experimentally compared the damping characteristics of original and aftermarket rear shock absorbers using a laboratory test rig with variable-speed and variable-stroke operation. Both specimens were tested at strokes of 60, 90, and 120 mm and excitation frequencies of 0.5–2.0 Hz, corresponding to peak piston velocities of 0.0942–0.7539 m/s. Maximum damping forces were measured using a force gauge, and the resulting force–velocity relationships were evaluated before and after modification of the test rig. Three-term sinusoidal functions were also fitted to the measured data using the MATLAB Curve Fitting Tool. Both shock absorbers exhibited nonlinear digressive behaviour, characterised by a rapid force increase at low-to-intermediate velocities followed by a stroke-dependent high-speed plateau. Matched-velocity comparisons showed that damping force varied with stroke even at approximately equal peak velocities, demonstrating that the response was not governed by piston velocity alone. Using the post-modification data, the aftermarket shock absorber generated an average damping force 15.8% higher than the original unit over the complete test matrix. Its peak force exceeded that of the original shock absorber by 29.4%, 9.8%, and 12.6% at strokes of 60, 90, and 120 mm, respectively. The corresponding apparent damping coefficients were also consistently higher for the aftermarket unit. These findings demonstrate that shock-absorber performance should be evaluated using experimentally determined force–velocity operating maps across multiple strokes and velocities rather than a single nominal damping coefficient.*

**Keywords:** *Automotive shock absorber; nonlinear damping; force–velocity characteristics; stroke dependence; experimental testing*

## 1. Introduction

Shock absorbers are essential components of vehicle suspension systems because they dissipate vibration energy generated by road irregularities and control the relative motion between the sprung and unsprung masses. Their damping characteristics affect suspension oscillation, tire–road contact, vehicle handling, and ride comfort. Consequently, accurate knowledge of the damping behaviour of a shock absorber is important for evaluating its condition, comparing different products, and selecting an appropriate component for a particular suspension application [1].

In simplified vibration and vehicle-dynamics analyses, a shock absorber is commonly represented as a linear viscous damper, in which the damping force is assumed to be directly proportional to the relative piston velocity. Although this representation is mathematically convenient, an actual hydraulic shock absorber exhibits a considerably more complex response. Its damping force may depend on piston velocity, displacement, excitation frequency, fluid pressure, valve configuration, fluid compressibility, friction, temperature, and internal geometry. Therefore, the response of a practical shock absorber generally cannot be represented adequately by a single constant damping coefficient [2]–[5]. Experimental studies have shown that damper force may vary with both velocity and displacement and can form closed hysteresis loops in force–velocity and force–displacement diagrams.

The complex behaviour of hydraulic shock absorbers has encouraged the development of various experimental procedures for determining their dynamic properties. Rao et al. [6] developed a testing and analysis method for obtaining equivalent stiffness and damping parameters under different excitation conditions. Talbott and Starkey [7] developed and experimentally validated a physical model of a high-performance monotube damper, including the effects of valve and fluid-flow characteristics. Boggs et al. [8] proposed an efficient empirical representation of a high-performance shock absorber based on measured data, while Cui et al. [9] developed a testing method specifically intended to identify nonlinear shock-absorber properties. These investigations demonstrate that experimental testing is necessary because shock-absorber characteristics cannot be determined reliably from nominal specifications or simplified theoretical assumptions alone.

The nonlinear damping force primarily results from the internal flow of hydraulic fluid through restricted passages, orifices, and valve assemblies. Changes in pressure difference and valve opening cause the slope of the force–velocity curve to vary over the operating range. Farjoud et al. [10] demonstrated that shim-stack geometry and orifice parameters strongly influence the nonlinear performance of monotube hydraulic dampers. Cui and Sun [11] experimentally identified nonlinear and hysteretic characteristics and represented them using an empirical hybrid model. Konieczny [12] further showed that damper characteristics may be oversimplified when damping force is treated only as a function of piston velocity. Barethiye et al. [13] similarly demonstrated that experimental automotive damper data exhibited both nonlinear force–velocity behaviour and hysteresis, requiring a combined representation to reproduce the measured response accurately.

Another important characteristic of practical shock absorbers is the difference between their compression and rebound responses. In many passive automotive dampers, the damping force produced during rebound is different from that generated during compression. This asymmetric response is associated with differences in fluid-flow paths and valve operation in the two directions of piston motion. Silveira et al. [14] showed that nonlinear asymmetric damping could produce vehicle responses different from those predicted using symmetric damping. Wang et al. [15] developed and experimentally validated a nonlinear physical model of a hydraulic damper that incorporated detailed valve and fluid effects. Ferdek and Łuczko [16] demonstrated that changes in internal flow passages could alter the force characteristics according to excitation amplitude, while Fernandes et al. [17] showed that damping asymmetry interacts with other suspension nonlinearities. These studies confirm that compression and rebound data should be evaluated separately when experimentally characterising a shock absorber.

The measured response may also differ substantially between individual shock absorbers because of differences in design, dimensions, valve settings, working-fluid condition, wear, manufacturing tolerance, and intended application. Even shock absorbers with similar external dimensions may generate different damping forces and exhibit different degrees of nonlinearity and asymmetry. An-Nizhami et al. [18] experimentally compared two shock absorbers and reported substantial differences in their measured damping forces. Tran et al. [19] distinguished linear, nonlinear, symmetric, and asymmetric shock-absorber characteristics and showed that each representation generated a different response. More recently, experimentally derived nonlinear damping relationships have been used to describe passive shock-absorber behaviour more realistically than conventional linear relationships [20]. Ata and Salem [21] also demonstrated that testing at different periodic excitations can reveal amplitude- and frequency-dependent hydraulic damper characteristics.

Although numerous analytical, empirical, and physical shock-absorber models have been developed, their parameters and characteristic curves are generally specific to the tested specimen and operating conditions. Therefore, data obtained for one shock absorber cannot automatically be used to describe another shock absorber. For the specimens considered in the present study, directly comparable experimental information obtained using the same test rig, measurement system, loading procedure, and data-processing method is required. Such a comparison is necessary to distinguish genuine differences between the shock absorbers from variations caused by the testing procedure.

Accordingly, this study experimentally investigates the nonlinear damping characteristics of two selected shock absorbers using a laboratory shock-absorber test rig. Both specimens are evaluated using consistent testing and measurement procedures so that their responses can be compared directly. The recorded force and motion data are analysed to determine the relationship between damping force and shock-absorber motion, with particular attention given to nonlinear behaviour, compression–rebound asymmetry, hysteresis, and differences between the two specimens.

The principal contribution of this study is therefore a comparative experimental assessment of the selected shock absorbers under identical test conditions. The study does not attempt to redesign the test rig or develop a numerical vehicle model. Instead, it focuses on identifying and comparing the actual damping responses measured from the two shock absorbers. The results are expected to provide a clearer understanding of their individual nonlinear characteristics and to demonstrate the importance of direct experimental testing when evaluating shock-absorber performance.

## 2. Material and Methodology

### 2.1. Study location, scope, and test specimens

The study was conducted at the Mechanical Engineering Workshop of Politeknik Negeri Semarang in 2025. The work focused on modifying a test rig for the rear shock absorbers of a Toyota Avanza to provide variable-speed and variable-stroke operation. The test specimens comprised an original shock absorber and an aftermarket shock absorber. Tests were conducted at stroke lengths of 60, 90, and 120 mm. For these stroke settings.

### 2.2. Equipment and instrumentation

The principal equipment consisted of the modified test rig, a 3 HP AC electric motor rated at 2850 rpm, an inverter for speed regulation, a 1:20 reduction gearbox, a crankshaft, a slider supported by linear bearings, and a shock-absorber mounting system secured by a snap pin. A force gauge was used to measure the damping force, a tachometer was used to measure shaft rotational speed, and a Miniature Circuit Breaker (MCB) provided electrical protection. Supporting fabrication equipment included a grinder, drilling machine, milling machine, and electric welding equipment.

### 2.3. Research workflow

The research workflow began with topic selection, identification and analysis of the test-rig problem, identification and analysis of the requirements, definition of the problem boundaries, and a literature review. A preliminary design concept was then developed and analysed. If the preliminary design was considered usable, a final design was prepared and the required components were inventoried. The subsequent stages comprised preparation of the work sequence, calculations and drawings, component procurement, fabrication of the apparatus, and a test-rig trial. If the apparatus did not operate as intended, failure analysis and corrective action were performed, with additional components procured where necessary. Once the apparatus operated satisfactorily, data were acquired and analysed, followed by vehicle-response simulation and formulation of the conclusions.

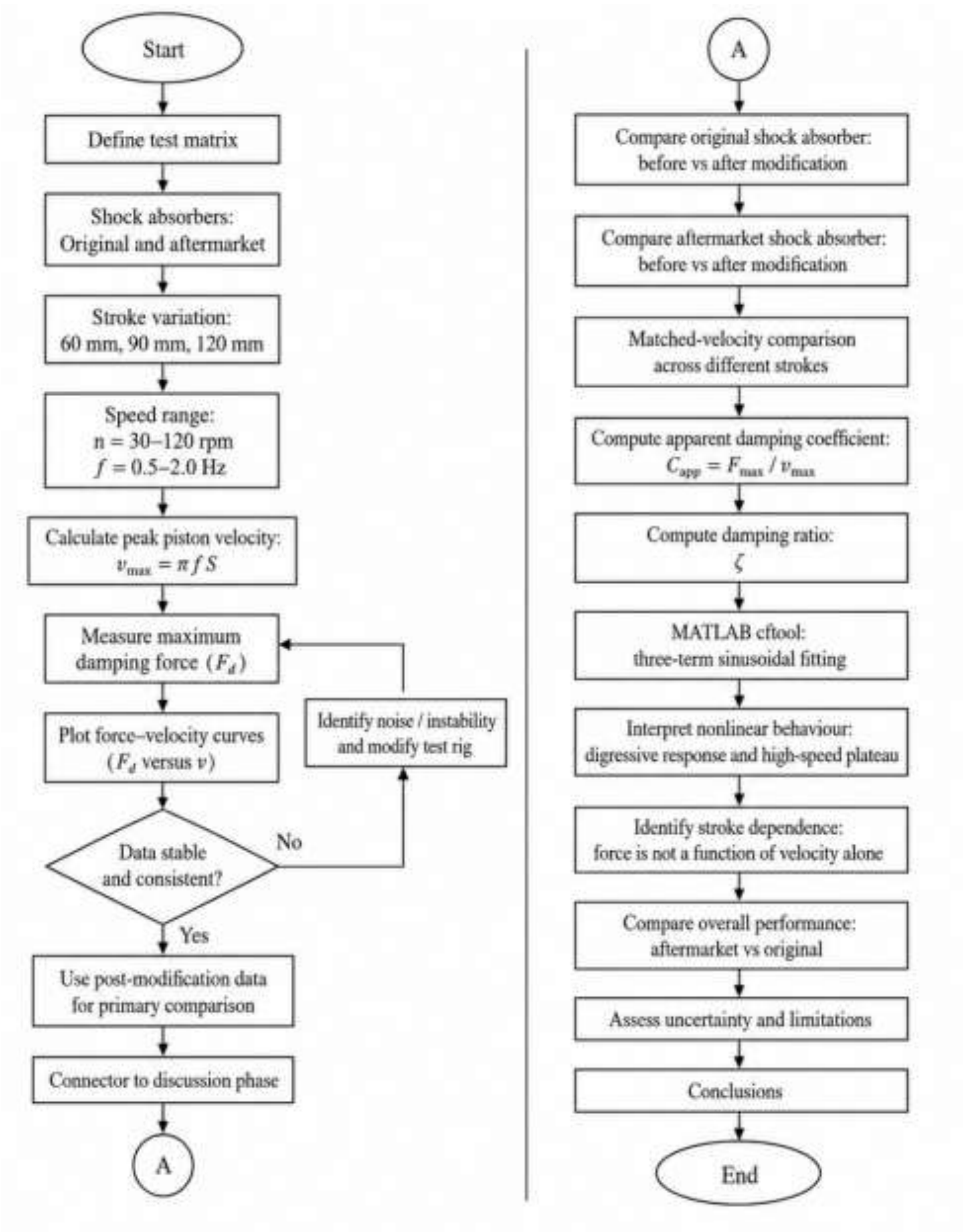


**Figure 1.** Research workflow diagram.

2.4. Test-rig design and operating principle

Figure 1 shows the shock-absorber test rig equipped with an inverter. The inverter controls the AC supply to regulate the rotational speed of the drive motor. An MCB is installed to limit the electrical current and protect the system against overload. The electric motor serves as the main drive, and its rotational motion is transmitted through the drive system to the crankshaft. The crankshaft converts rotational motion into reciprocating translational motion at the selected stroke. This motion drives the lower jaw of the test rig vertically upward and downward. Two linear bearings support and guide the lower jaw, enabling precise translational motion. The mechanism was intended to provide smooth and stable jaw movement so that the shock absorber could be tested effectively and accurately.

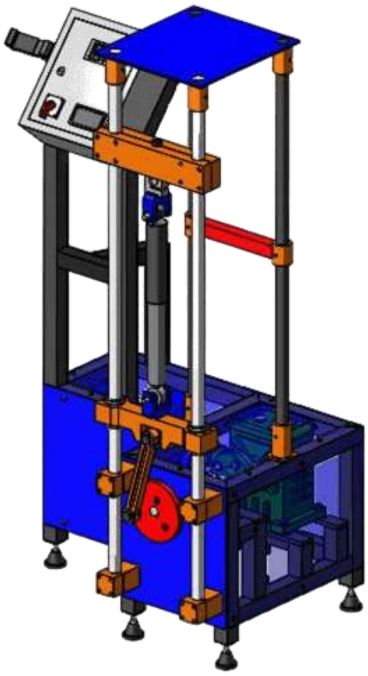

**Figure 2.** Test Rig Design.

2.5. Experimental procedure

The test rig was used to evaluate the performance and effectiveness of the shock absorbers in attenuating vibration. During testing, the shock absorber was subjected to repeated vertical upward and downward motion to simulate road-induced excitation. The operating speed was varied to observe the damper response to dynamic loading at different speed levels. This procedure was intended to support analysis of the ability of the shock absorber to contribute to vehicle stability and ride comfort.

1. Connect the machine power cable to the electrical supply.
2. Set the MCB in the control panel to the ON position.
3. Turn on the main power switch (callout 1 in Figure 3).
4. Set the required stroke length (callout 2 in Figure 3).
5. Install the shock absorber and secure it using the snap pin.
6. Turn on the inverter (callout 3 in Figure 3).
7. Turn on the force gauge, set the measurement unit to Newtons, press Peak to display the maximum value, and press Zero to reset the initial reading (callout 5 in Figure 3).
8. Adjust the motor speed using the inverter and observe the damping force on the force-gauge display.
9. Verify the rotational speed using the tachometer (callout 4 in Figure 3).
10. Repeat the preceding steps whenever the stroke setting is changed.

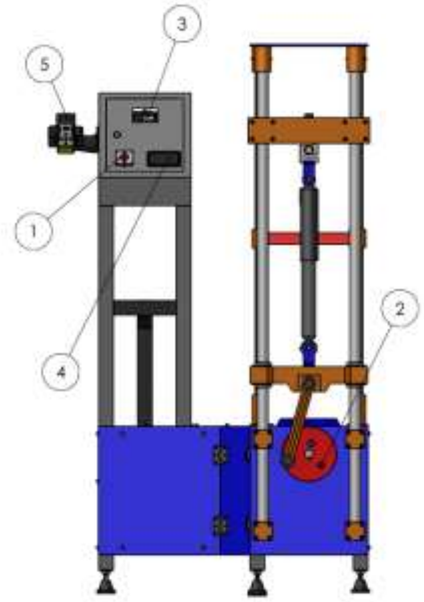


**Figure 3.** Test Rig Components.

## 3. Results and discussion

### 3.1. Test matrix and basis for interpretation

The two shock absorbers were tested at rotational speeds n of 30-120 rpm, corresponding to excitation frequencies f of 0.5-2.0 Hz, and at full strokes S of 60, 90, and 120 mm. For a sinusoidal actuator displacement, the peak piston velocity is v_max = pi f S, where S is expressed in metres. The resulting velocity range was 0.0942-0.7539 m/s. The selected matrix therefore covers a broad low-to-high damper-speed range while also providing several overlapping velocity points obtained with different combinations of stroke and frequency. These overlaps are useful because they allow a preliminary assessment of whether damping force is controlled by velocity alone or also depends on displacement amplitude and loading history. The frequency and amplitude ranges are also broadly comparable with laboratory characterisation ranges reported for hydraulic dampers, although direct numerical comparison between different damper constructions should be made cautiously [3], [21], [22].

**Table 1.** Excitation matrix and calculated peak piston velocities.

| n (rpm) | f (Hz) | v_max at S=60 mm (m/s) | v_max at S=90 mm (m/s) | v_max at S=120 mm (m/s) |
|---|---|---|---|---|
| 30 | 0.50 | 0.0942 | 0.1414 | 0.1885 |
| 45 | 0.75 | 0.1414 | 0.2120 | 0.2827 |
| 60 | 1.00 | 0.1885 | 0.2827 | 0.3770 |
| 75 | 1.25 | 0.2356 | 0.3534 | 0.4712 |
| 90 | 1.50 | 0.2827 | 0.4241 | 0.5655 |
| 105 | 1.75 | 0.3299 | 0.4948 | 0.6597 |
| 120 | 2.00 | 0.3770 | 0.5655 | 0.7539 |

The tables report only the magnitude of the maximum damping force for each test condition. In Figures 3-6, these magnitudes were assigned opposite signs to construct nominal compression and rebound branches, with positive velocity representing rebound and negative velocity representing compression. Consequently, the figures demonstrate the nonlinear magnitude of the force-velocity relationship, but they do not contain independently measured compression and rebound branches. The apparent symmetry about the origin should therefore be interpreted as a plotting convention rather than evidence that the physical dampers are symmetric. A genuine assessment of compression-rebound asymmetry, hysteresis, or energy dissipation would require cycle-resolved force, velocity, and displacement histories.

The terms 'before' and 'after' refer to modification of the test rig, not modification of the shock absorbers. The pre- and post-modification measurements are therefore treated here as a sensitivity check on the experimental arrangement. The post-modification data are used as the primary basis for comparing the two shock absorbers because these curves show fewer high-speed reversals and more clearly defined plateaus. Nevertheless, no repeated-test statistics or measurement uncertainty were supplied, so improved precision cannot be established quantitatively from curve smoothness alone.

3.2. Nonlinear response of the original shock absorber

Figure 3 plots damping force F_d against piston velocity v for the original shock absorber at strokes of 60, 90, and 120 mm, before and after modification of the test rig. All six curves exhibit an S-shaped force-velocity relationship: the force rises rapidly through the low- and intermediate-speed region and then approaches a stroke-dependent plateau. This digressive behaviour is typical of hydraulic dampers in which restricted bleed flow controls the low-speed response, whereas progressive opening of the main valve or shim stack increases the effective flow area at higher speed and reduces the incremental force gradient. Similar transitions between low- and high-speed force gradients have been described in experimentally validated damper models [7], [10].

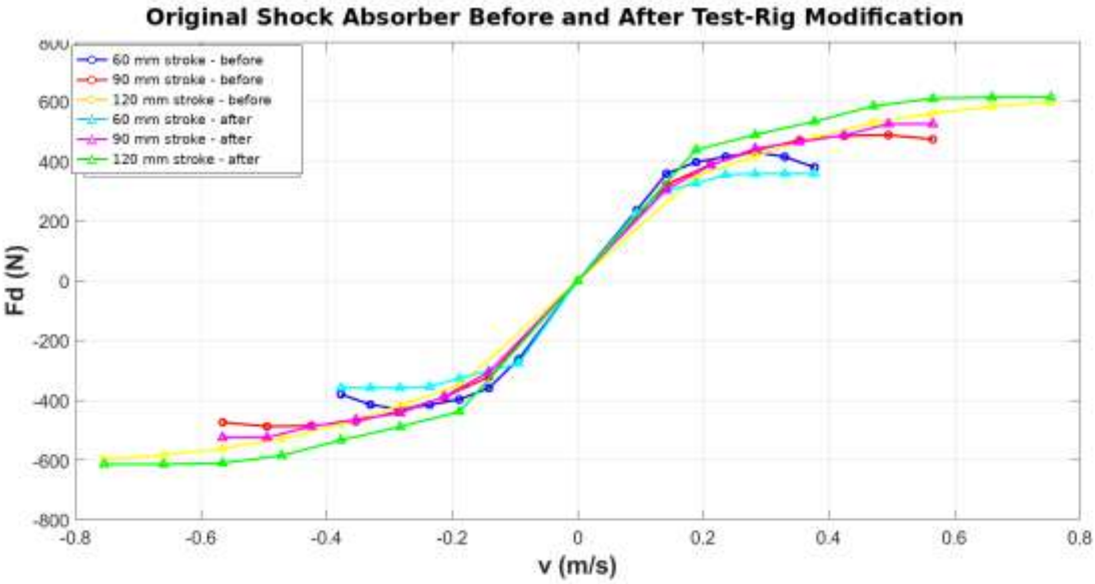


**Figure 4**. Measured damping-force magnitude versus piston velocity for the original shock absorber before and after modification of the test rig. The negative branch is a sign-reversed representation of the reported force magnitudes, not an independently measured compression branch.

For the post-modification configuration, the force at the 60 mm stroke increased from 227.4 N at 0.0942 m/s to 358.4 N at 0.2827 m/s and then remained constant up to 0.3770 m/s. At the 90 mm stroke, the force increased from 305.9 N at 0.1414 m/s to 525.0 N at 0.4948 m/s, after which no further increase was measured. The 120 mm stroke generated the largest force, rising from 438.5 N at 0.1885 m/s to 614.5 N at 0.6597 m/s and remaining at that level at 0.7539 m/s. The progressive reduction in slope at high velocity indicates that the damper is not well represented by a single linear coefficient. Instead, the effective flow resistance decreases as the internal valve system opens, producing a force increase that is sublinear with velocity.

The pre-modification curves contain two notable high-speed reversals. At the 60 mm stroke, the force reached 430.9 N at 0.2827 m/s but decreased to 380.0 N at 0.3770 m/s, a reduction of 11.8%. At the 90 mm stroke, the force decreased from 487.9 N at 0.4948 m/s to 473.9 N at 0.5655 m/s. Such decreases may reflect genuine hydraulic effects, including aeration, cavitation, temperature-dependent viscosity, or transient valve behaviour, but they may also arise from speed fluctuation, structural vibration, or signal-processing limitations in the original rig configuration. The disappearance of the strongest reversal after modification is consistent with improved actuation stability; however, this interpretation remains qualitative because no repeated cycles, temperature records, or confidence intervals were reported.

The overlapping velocity points reveal an additional dependence on the imposed stroke. At v_max approximately equal to 0.2827 m/s, the post-modification force was 358.4 N for the 60 mm stroke, 442.9 N for the 90 mm stroke, and 488.9 N for the 120 mm stroke. Thus, even at nearly identical peak velocity, increasing the stroke from 60 to 90 and 120 mm increased the measured force by 23.6% and 36.4%, respectively. A similar difference is observed at v_max approximately equal to 0.5655 m/s, where the 120 mm-stroke force exceeded the 90 mm value by 16.3%. These matched-velocity comparisons demonstrate that the response is not a single-valued function of peak velocity. Possible causes include displacement-sensitive valving, gas-volume compression, seal friction, fluid compressibility, and differences in pressure history over the cycle. This observation agrees with studies showing that velocity-only damper descriptions can omit important dynamic effects [2], [12], [13].

Figure 4 presents the three-term sinusoidal functions fitted to the original-damper data using the MATLAB Curve Fitting Tool. The fitted curves reproduce the measured S-shaped trend within the tested interval and provide a continuous interpolation between the discrete velocity points. The fits should, however, be regarded as empirical interpolation functions rather than physical damper models. The results does not report R-squared, RMSE, residual distributions, parameter confidence bounds, or independent validation data. Accordingly, the apparent agreement in Figure 4 is insufficient to demonstrate predictive accuracy, particularly outside the measured range.

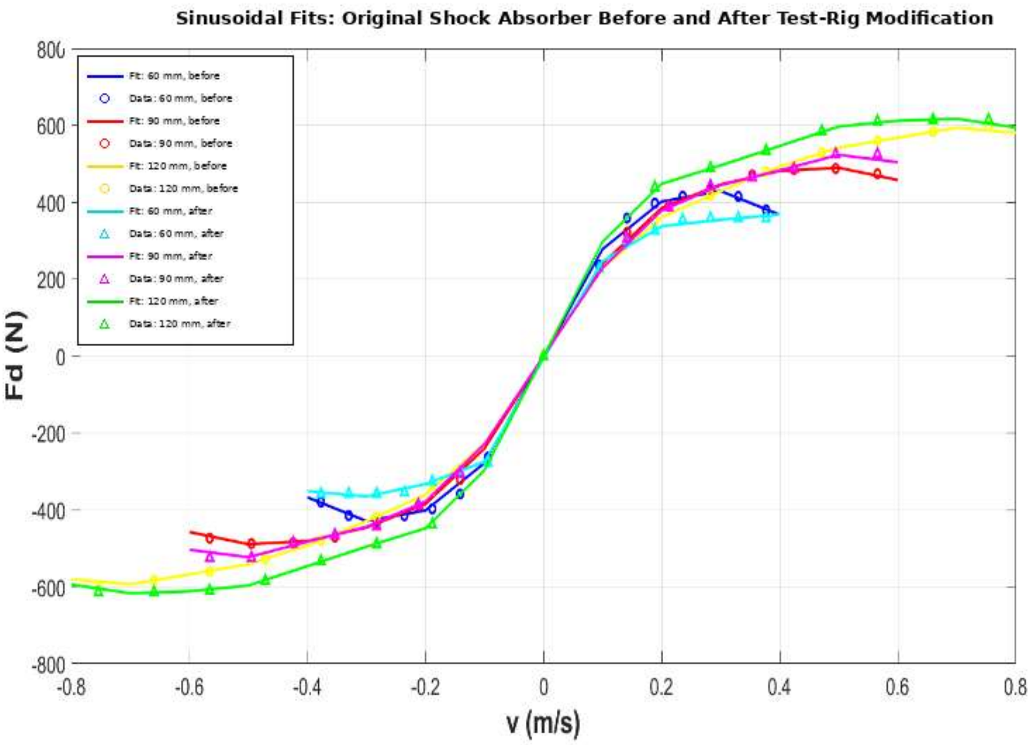


**Figure 5.** Three-term sinusoidal fits to the original-shock-absorber force-velocity data before and after test-rig modification.

3.3. Nonlinear response of the aftermarket shock absorber

Figure 5 shows the corresponding force-velocity curves for the aftermarket shock absorber. As for the original component, the overall response is strongly nonlinear and digressive, with a steep central region followed by a high-speed plateau. The post-modification maximum forces were 463.9, 576.4, and 692.0 N for strokes of 60, 90, and 120 mm, respectively. The plateau was reached at approximately 0.2827 m/s for the 60 mm stroke, 0.4241 m/s for the 90 mm stroke, and 0.6597 m/s for the 120 mm stroke. The increasing plateau level with stroke indicates that the internal force response depends on the operating path and not only on instantaneous velocity.

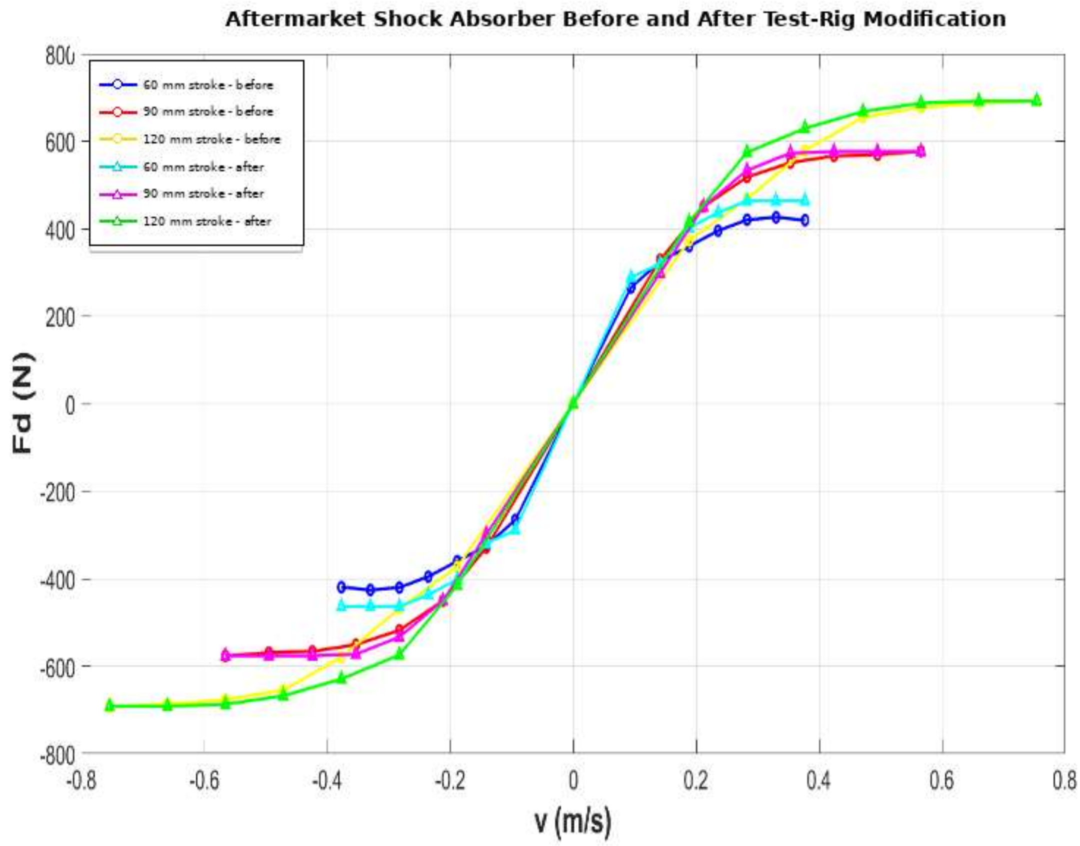


**Figure 6.** Measured damping-force magnitude versus piston velocity for the aftermarket shock absorber before and after modification of the test rig. The negative branch is a sign-reversed representation of the reported force magnitudes.

The effect of the rig modification was not a uniform force increase. Averaged over the seven speed points, the post-modification forces changed by +8.4%, approximately 0.1%, and +6.7% at strokes of 60, 90, and 120 mm, respectively. The largest individual change occurred at the lowest speed of the 120 mm test, where the measured force increased from 372.9 to 415.4 N. At the highest speed, the 120 mm force was unchanged at 692.0 N. This pattern suggests that the modification primarily affected low- and intermediate-speed measurement or actuation conditions rather than the ultimate high-speed force capacity of the damper. However, without repeat tests it is not possible to separate rig-related changes from temperature drift, conditioning of the working fluid, or specimen-to-specimen variability.

The matched-velocity comparison again confirms amplitude dependence. At v_max approximately equal to 0.2827 m/s, the post-modification forces were 463.9, 533.5, and 574.5 N for strokes of 60, 90, and 120 mm, respectively. Relative to the 60 mm stroke, the 90 and 120 mm forces were higher by 15.0% and 23.8%. At v_max approximately equal to 0.5655 m/s, increasing the stroke from 90 to 120 mm increased the force from 576.4 to 687.0 N, or 19.2%. These differences are too large to be attributed to rounding of the velocity values and indicate that a velocity-only curve cannot uniquely describe this damper over the full test matrix.

Figure 6 shows the sinusoidal fits for the aftermarket damper. The fits capture the measured nonlinear trend visually, but several reported coefficient sets contain very large terms of similar magnitude and opposite phase. Such cancellation is a common indication of parameter non-uniqueness and can produce an apparently accurate interpolation while remaining highly sensitive to small changes in the data. The functions should therefore not be extrapolated beyond -0.7539 to 0.7539 m/s or used directly in time-domain simulation without reporting goodness-of-fit metrics and validating them against independent cycles. More robust alternatives for subsequent modelling include monotone piecewise functions, restoring-force surfaces, hysteresis models, or physically based valve-flow formulations [10], [13], [22].

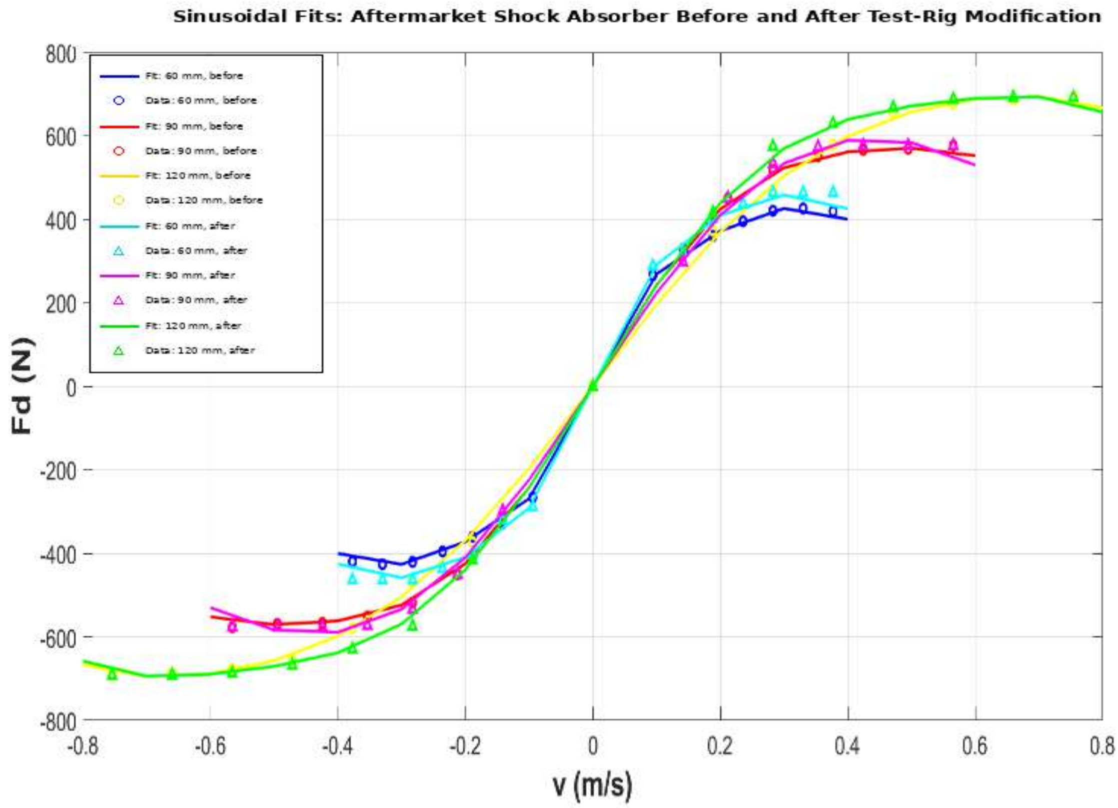


**Figure 7.** Three-term sinusoidal fits to the aftermarket-shock-absorber force-velocity data before and after test-rig modification.

3.4. Comparison between the original and aftermarket shock absorbers

Using the post-modification data as the common comparison basis, the aftermarket shock absorber generated a higher mean force over the complete 21-point matrix: 513.4 N compared with 443.3 N for the original damper, corresponding to an increase of 15.8%. The difference was not uniform over the operating range. At the lowest tested velocity, the aftermarket force was 2.5% lower than the original value for the 90 mm stroke and 5.3% lower for the 120 mm stroke. As velocity increased, the aftermarket force became consistently higher. This crossover suggests comparatively compliant low-speed behaviour combined with stronger medium- and high-speed valving, rather than a simple uniform increase in damping.

**Table 2**. Peak-force summary. The last column compares post-modification peak forces at the same stroke.

| Damper | Stroke (mm) | Pre-modification peak force (N) | Velocity at pre peak (m/s) | Post-modification peak force (N) | Velocity at post peak (m/s) | Post aftermarket-original difference (%) |
|---|---|---|---|---|---|---|
| Original | 60 | 430.9 | 0.2827 | 358.4 | 0.2827 | - |
| Original | 90 | 487.9 | 0.4948 | 525.0 | 0.4948 | - |
| Original | 120 | 597.4 | 0.7539 | 614.5 | 0.6597 | - |
| Aftermarket | 60 | 426.0 | 0.3299 | 463.9 | 0.2827 | 29.4 |
| Aftermarket | 90 | 577.0 | 0.5655 | 576.4 | 0.4241 | 9.8 |
| Aftermarket | 120 | 692.0 | 0.7539 | 692.0 | 0.6597 | 12.6 |

The peak-force advantage of the aftermarket unit was largest at the 60 mm stroke, where its post-modification plateau of 463.9 N exceeded the original value of 358.4 N by 29.4%. The corresponding differences at 90 and 120 mm were 9.8% and 12.6%. These results imply that the distinction between the dampers is most pronounced in the shorter-stroke operating regime. For design interpretation, this means that ranking the two shock absorbers using only one stroke or one velocity could be misleading; the comparison must be made over an operating map.

The results calculated an apparent damping coefficient by averaging the pointwise ratios $F_{max} / v_{max}$ for the post-modification data. This produces 1584.04, 1430.31, and 1362.61 N s/m for the original damper and 1941.41, 1612.41, and 1500.65 N s/m for the aftermarket damper at strokes of 60, 90, and 120 mm, respectively. The aftermarket values are higher by 22.6%, 12.7%, and 10.1%. For both dampers, however, the apparent coefficient decreases as stroke increases: by 14.0% for the original unit and 22.7% for the aftermarket unit between 60 and 120 mm. This decrease follows directly from the digressive curves, because force grows more slowly than velocity once the valve system enters its high-flow regime.

**Table 3.** Apparent damping coefficients and damping ratios calculated from the post-modification data.

| Stroke (mm) | C app original (N s/m) | C app aftermarket (N s/m) | Difference (%) | zeta original | Zeta aftermarket | Interpretation |
|---|---|---|---|---|---|---|
| 60 | 1584.04 | 1941.41 | 22.56 | 0.21 | 0.24 | Largest separation |
| 90 | 1430.31 | 1612.41 | 12.73 | 0.19 | 0.20 | Moderate separation |
| 120 | 1362.61 | 1500.65 | 10.13 | 0.18 | 0.18 | Similar system-level ratio |

These averaged values should not be interpreted as constant viscous coefficients. They combine measurements from different velocities and do not represent the local slope dF_d/dv, the area of a force-displacement loop, or an equivalent coefficient derived from dissipated energy. Their dependence on stroke is itself evidence that a single C value is inadequate. The values are nevertheless useful as compact comparative indicators when their calculation method and velocity range are stated explicitly.

Using the stated supported mass of 550 kg and spring stiffnesses of 25,000 and 30,000 N/m, the critical damping coefficients are approximately 7416.2 and 8124.0 N s/m, respectively. The resulting damping ratios decrease from 0.21 to 0.18 for the original system and from 0.24 to 0.18 for the aftermarket system as stroke increases. The convergence at the 120 mm stroke does not mean that the two dampers generate the same force; rather, the higher force of the aftermarket damper is normalised by a higher assumed critical damping coefficient. Because damping ratio is a property of the combined mass-spring-damper system, it should not be used as an intrinsic shock-absorber property unless both dampers are evaluated with the same vehicle mass and suspension stiffness. Previous experimental comparisons have likewise shown that reported damping ratios depend strongly on the selected specimen and system assumptions [18].

### 3.5. Reliability, limitations, and implications

The main result of the study is that both shock absorbers exhibit nonlinear, digressive, and stroke-dependent force-velocity characteristics, while the aftermarket unit generally produces higher damping force in the medium- and high-speed regions. The matched-velocity comparisons are particularly important because they demonstrate that the force cannot be represented uniquely by peak velocity. This conclusion is consistent with the established roles of fluid compressibility, valve dynamics, friction, aeration, and pressure-history effects in hydraulic dampers [2], [12], [13].

Several limitations should be stated explicitly. First, results do not report replicate tests, cycle-to-cycle scatter, sensor calibration, sampling frequency, filtering settings, fluid temperature, or preload. Therefore, the magnitude of random and systematic uncertainty cannot be quantified, and the effect of the rig modification cannot be separated rigorously from specimen conditioning or thermal drift. Second, only peak force magnitudes are tabulated. Because the positive and negative branches are constructed symmetrically, the present data cannot support conclusions about compression-rebound asymmetry, hysteresis-loop area, phase lag, or dissipated energy per cycle. Third, testing one original and one aftermarket specimen does not establish the variability of the corresponding product populations.

The experimental design also couples stroke, frequency, and velocity. Although overlapping velocity points provide evidence of amplitude dependence, the individual effects of stroke and frequency cannot be fully separated without a factorial test plan that varies one quantity while holding the others constant. Finally, the three-term sinusoidal functions provide flexible interpolation but are not physically constrained and may become oscillatory outside the calibration interval. Future reporting should include repeated cycles, uncertainty bars, temperature control, separate compression and rebound measurements, force-displacement loops, energy dissipation, and independent validation of any fitted model.

Within these limitations, the results have a clear practical implication: selecting or modelling a shock absorber using a single nominal damping coefficient can obscure both its high-speed saturation and its dependence on stroke. The aftermarket component cannot simply be described as uniformly 'stiffer'; it is slightly softer at a few lowest-speed conditions but generates substantially greater force over most of the medium- and high-speed range. Consequently, component comparison and subsequent suspension modelling should use an experimentally defined operating map rather than a single coefficient or one isolated test point.

## 4. Conclusions

This study experimentally investigated the nonlinear characteristics of original and aftermarket rear shock absorbers using a laboratory test rig with variable stroke and operating speed. Both shock absorbers exhibited nonlinear, digressive force–velocity behavior, characterized by a rapid increase in damping force at low-to-intermediate piston velocities followed by a gradual high-speed plateau. The matched-velocity comparisons further showed that damping force was affected by stroke amplitude and could not be represented adequately as a function of piston velocity alone. This finding confirms that a single constant viscous damping coefficient is insufficient to describe the tested shock absorbers over the full operating range.

Using the post-modification data as the primary comparison basis, the aftermarket shock absorber generated an average damping force approximately 15.8% higher than that of the original shock absorber over the complete test matrix. Its peak damping force exceeded that of the original component by approximately 29.4%, 9.8%, and 12.6% at strokes of

60, 90, and 120 mm, respectively. The corresponding apparent damping coefficients were 1941.41, 1612.41, and 1500.65 N·s/m for the aftermarket shock absorber, compared with 1584.04, 1430.31, and 1362.61 N·s/m for the original unit. Nevertheless, the aftermarket component was not uniformly more highly damped at all operating points, because slightly lower forces were observed at several low-speed conditions. It is therefore more accurate to describe the aftermarket shock absorber as having stronger medium- and high-speed damping rather than simply being uniformly stiffer.

Modification of the test rig produced smoother force–velocity trends and reduced several high-speed force reversals observed in the initial measurements, indicating improved actuation and measurement stability. However, the absence of repeated tests, uncertainty estimates, temperature monitoring, and cycle-resolved force and displacement data prevents a rigorous quantitative assessment of repeatability, hysteresis, compression–rebound asymmetry, and dissipated energy. The sinusoidal equations obtained using MATLAB provide continuous interpolation within the measured velocity range, but they should not be extrapolated or treated as physically based damper models without further validation.

Overall, the results demonstrate that shock-absorber evaluation should be conducted over a range of strokes and velocities rather than at a single operating point. An experimentally determined force–velocity operating map provides a more representative basis for comparing shock absorbers and for their subsequent implementation in suspension models. Future studies should incorporate repeated measurements, uncertainty analysis, controlled fluid temperature, independent compression and rebound measurements, and force–displacement hysteresis loops to achieve a more complete characterization of nonlinear damping behavior. The experimental arrangement and test procedure supporting these conclusions are described in the revised Methodology section.

**References**


[1] Dixon, J. C. (2007). The Shock Absorber Handbook (2nd ed.). John Wiley & Sons.

[2] Duym, S., Stiens, R., and Reybrouck, K. (1997). Evaluation of shock absorber models. Vehicle System Dynamics, 27(2), 109–127. https://doi.org/10.1080/00423119708969325.

[3] Basso, R. (1998). Experimental characterization of damping force in shock absorbers with constant velocity excitation. Vehicle System Dynamics, 30(6), 431–442. https://doi.org/10.1080/00423119808969459.

[4] Duym, S. W. R. (2000). Simulation tools, modelling and identification for an automotive shock absorber in the context of vehicle dynamics. Vehicle System Dynamics, 33(4), 261–285.

[5] Lee, C. T., and Moon, B. Y. (2006). Simulation and experimental validation of vehicle dynamic characteristics for displacement-sensitive shock absorber using fluid-flow modelling. Mechanical Systems and Signal Processing, 20(2), 373–388. https://doi.org/10.1016/j.ymssp.2004.09.006.

[6] Rao, M. D., Gruenberg, S., and Torab, H. (1999). Measurement of dynamic properties of automotive shock absorbers for NVH. SAE Technical Paper 1999-01-1840. https://doi.org/10.4271/1999-01-1840.

[7] Talbott, M. S., and Starkey, J. (2002). An experimentally validated physical model of a high-performance mono-tube damper. SAE Technical Paper 2002-01-3337. https://doi.org/10.4271/2002-01-3337.

[8] Boggs, C., Ahmadian, M., and Southward, S. (2010). Efficient empirical modelling of a high-performance shock absorber for vehicle dynamics studies. Vehicle System Dynamics, 48(4), 481–505. https://doi.org/10.1080/00423110902906292.

[9] Cui, Y., Kurfess, T. R., and Messman, M. (2010). Testing and modeling of nonlinear properties of shock absorbers for vehicle dynamics studies. In Proceedings of the World Congress on Engineering and Computer Science 2010, Vol. II, pp. 949–954.

[10] Farjoud, A., Ahmadian, M., Craft, M., and Burke, W. (2012). Nonlinear modeling and experimental characterization of hydraulic dampers: Effects of shim stack and orifice parameters on damper performance. Nonlinear Dynamics, 67(2), 1437–1456. https://doi.org/10.1007/s11071-011-0079-2.

[11] Cui, Y., and Sun, F. (2013). Empirical modeling of nonlinear and hysteresis characteristics of the shock absorber. High Technology Letters, 19(3), 267–272. https://doi.org/10.3772/j.issn.1006-6748.2013.03.008.

[12] Konieczny, Ł. (2016). Analysis of simplifications applied in vibration damping modelling for a passive car shock absorber. Shock and Vibration, 2016, Article 6182847. https://doi.org/10.1155/2016/6182847.

[13] Barethiye, V., Pohit, G., and Mitra, A. (2017). A combined nonlinear and hysteresis model of shock absorber for quarter car simulation on the basis of experimental data. Engineering Science and Technology, an International Journal, 20(6), 1610–1622. https://doi.org/10.1016/j.jestch.2017.12.003.

[14] Silveira, M., Pontes, B. R., and Balthazar, J. M. (2014). Use of nonlinear asymmetrical shock absorber to improve comfort on passenger vehicles. Journal of Sound and Vibration, 333(7), 2114–2129. https://doi.org/10.1016/j.jsv.2013.12.001.

[15] Wang, W. L., Zhou, Z., Yu, D., Qin, Q., and Iwnicki, S. (2017). Rail vehicle dynamic response to a nonlinear physical "in-service" model of its secondary suspension hydraulic dampers. Mechanical Systems and Signal Processing, 95, 138–157. https://doi.org/10.1016/j.ymssp.2017.03.031.

[16] Ferdek, U., and Łuczko, J. (2018). Nonlinear modeling and analysis of a shock absorber with a bypass. Journal of Theoretical and Applied Mechanics, 56(3), 615–629. https://doi.org/10.15632/jtam-pl.56.3.615.

[17] Fernandes, J. C. M., Gonçalves, P. J. P., and Silveira, M. (2020). Interaction between asymmetrical damping and geometrical nonlinearity in vehicle suspension systems improves comfort. Nonlinear Dynamics, 99, 1561–1576. https://doi.org/10.1007/s11071-019-05374-y.

[18] An-Nizhami, A., Sriyanto, N. B., Sumiyarso, B., Ulum, S. N., Riadini, E. R., and Widodo, I. G. (2023). Experimental and numerical study of shock absorber characterization and the implication on the dynamics of a half-vehicle suspension system model. Jurnal Rekayasa Mesin, 18(3), 409–418. https://doi.org/10.32497/jrm.v18i3.5023.

[19] Tran, H. N., Gunawan, F. E., and Pham, N. D. (2023). Influence of a nonlinear asymmetric shock absorber on vibration of a bus subjected to harmonic excitation. Journal of Vibroengineering, 26(1), 128–138. https://doi.org/10.21595/jve.2023.23404.

[20] An-Nizhami, A., Herlambang, Y. D., Apriandi, N., Bono, Sugiono, F. A. F., Sai'in, A., Widodo, I. G., and Yanuar, P. (2025). Modeling the dynamics of a passenger car using experimental data on nonlinear passive shock absorbers. Automotive Experiences, 8(1), 32–45. https://doi.org/10.31603/ae.12792.

[21] Ata, W. G., and Salem, A. M. (2025). Experimental characterisation and nonparametric modeling of an armoured-vehicle hydraulic shock absorber under periodic excitations. Journal of Vibration Engineering & Technologies, 13, Article 311. https://doi.org/10.1007/s42417-025-01830-9.

[22] Titurus, B., du Bois, J., Lieven, N., and Hansford, R. E. (2010). A method for the identification of hydraulic damper characteristics from steady velocity inputs. Mechanical Systems and Signal Processing, 24(8), 2868–2887.